A comprehensive pharmacological survey across heterogeneous patient-derived GBM stem cell models.

Richard J.R. Elliott[1], Peter Nagle[1], Muhammad Furqan[1], John C. Dawson[1], Aoife McCarthy[1], Alison F Munro[1], Camilla Drake[1], Gillian M Morrison[2], Michael Marand[1], Daniel Ebner[3], Steven M. Pollard[2], Valerie G Brunton[1], Margaret C Frame[1] and Neil O. Carragher[1]

[1]Edinburgh Cancer Research, Institute of Genetics and Cancer, University of Edinburgh, Western General Hospital, Edinburgh, UK. Cancer Research UK Scotland Centre, UK

[2]Institute of Regeneration and Repair, Cancer Research UK Scotland Centre, University of Edinburgh, UK, EH16 4UU

[3]Nuffield Dept. Of Medicine, University of Oxford, Old Road Campus, Oxford OX3 7BN, U.K.

Address for correspondence:

Prof Neil Carragher:

Edinburgh Cancer Research,

Institute of Genetics and Cancer,

University of Edinburgh,

Western General Hospital,

Edinburgh, UK. EH4 2XR

Tel: +44 (0)131 6518671

Email: n.carragher@ed.ac.uk

Abstract

Despite substantial drug discovery investments, the lack of any significant therapeutic advancement in the treatment of glioblastoma (GBM) over the past two decades calls for more innovation in the identification of effective treatments. The inter- and intra-patient heterogeneity of GBM presents significant obstacles to effective clinical progression of novel treatments by contributing to tumour plasticity and rapid drug resistance that confounds contemporary target directed drug discovery strategies. Phenotypic drug screening is ideally suited to heterogeneous diseases, where targeting specific oncogenic drivers have been broadly ineffective. Our hypothesis is that a modern phenotypic led approach using disease relevant patient derived GBM stem cell systems will be the most productive approach to identifying new therapeutic targets, drug classes and future drug combinations that target the heterogeneity of GBM. In this study we incorporate a panel of patient derived GBM stem cell lines into an automated and unbiased 'Cell Painting' assay to quantify multiple GBM stem cell phenotypes. By screening several compound libraries at multiple concentrations across a panel of patient-derived GBM stem cells we provide the first comprehensive survey of distinct pharmacological classes and known druggable targets, including all clinically approved drug classes and oncology drug candidates upon multiple GBM stem cell phenotypes linked to cell proliferation, survival and differentiation. Our data set representing, 3866 compounds, 2.2million images and 64000 datapoints is the largest phenotypic screen carried out to date on a panel of patient-derived GBM stem cell models that we are aware off. We seek to identify agents and targets classes which engender potent activity across heterogenous GBM genotypes and phenotypes, in this study we further characterize two validated target classes, histone deacetylase inhibitors and cyclin dependent kinases that exert broad and potent effects on the phenotypic and transcriptomic profiles of GBM stem cells. Here we present all validated hit compounds and their target assignments for the GBM community to explore.

Introduction

Glioblastoma (GBM), a Grade IV astrocytoma, is a highly complex disease that remains difficult to treat. Mortality rates in the UK have increased over the last 30 years, especially in the over 60 age group, as incidence rates outpace survival improvements [1] . GBM is therefore the most common and aggressive primary malignant tumour of the brain and represents an urgent area of unmet medical need. Since the introduction of post-surgical, concomitant radiotherapy and adjuvant temozolomide in 2005 (the 'Stupp protocol'), which increased median overall survival by ~3 months[2], a lack of effective, novel treatments for GBM have been introduced into broad clinical use and 5 year survival rates from time of diagnosis remain at less than 5%[3]. Clinical and scientific research over the last 20 years has revealed a complex landscape of remarkable intra- and inter-tumoral heterogeneity associated with the highly dynamic nature of GBM molecular biology [4, 5{Verhaak, 2010 #312{Brennan, 2013 #313]. The complex biology driving the disease is further exacerbated by the addition of GBM stem cells (GSC), driving self-renewal and resistance mechanisms[6-11]. The self-renewing capacity of GSCs is an inherent feature of GBM to which the tumour microenvironment, or the GBM stem cell niche, contributes by supporting adaptive signal rewiring, heterogeneous tumour evolution and therapeutic resistance[12, 13]. Phospho-proteomic studies performed on patient derived GBM model systems demonstrates rapid rewiring of pathway signalling at the post-translational pathway level following effective inhibition of some of the most compelling drug targets such as the mTOR pathway, that is hyperactivated in approximately 90% of GBM[14]. GBM plasticity and heterogeneity thus confound modern target-based drug discovery strategies contributing to drug resistance and relapse, hence the targeting of clear oncogenic drivers of GBM, such as EGFR amplification/mutation or RAS, PI3K signalling, has not translated into significant efficacy in GBM clinical management. Emerging single-cell transcriptomic[15], proteomic[16] and image-based phenotypic screening[17] technologies combined with improved patient-derived GSC models[18] provide new opportunities to understand and overcome disease heterogeneity. New hope for the development of novel therapeutic classes and drug combinations that may overcome some if this heterogeneity and support new personalized treatments strategies for GBM is provided from the recent phase 2 ROAR basket clinical trial study evaluating a combination a the BRAF targeting agent (dabrafenib) and the MEK inhibitor (trametinib) which includes a cohort of 45 high grade glioma (HGG, including GBM) patients with BRAFV600E mutation. The primary endpoint of, investigator-assessed overall response rate was 33% in the HGG cohort. Secondary endpoints of median duration of response (DoR), progression-free survival (PFS) and median overall survival (OS) in the HGG cohort was; 31.2, 5.5 and 17.6 months respectively[19]. Emerging case reports from both adult and pediatric patients also point to the benefit of treating BRAF mutation-positive glioblastoma and gliomas with the dabrafenib and trametinib combination[20-23]. However, BRAF V600E mutation can be found in approximately only 3% of GBM patients therefore, while such personalized treatments offer hope, the challenge is addressing the majority of patients which do not fall into molecular subtypes defined by a well-established druggable target or pathway or are refractory to such personalized treatments.

The drug development of imidazotetrazines, such as temozolomide, extended from chemocentric and phenotypic-led collaborative research exploring the *in vitro* and *in vivo* anti-cancer properties of small molecules, dacarbazine and mitozolomide (azolastone)[24] emphasizing the value of incorporating complex tumour biology into early stage drug design and selection. Phenotypic drug discovery (PDD), defined as the identification of hit or lead compounds prior to target identification[25], has historically contributed more than target based drug discovery (TDD), in terms of first-in-class drugs approved by the FDA since 1999[26, 27], yet TDD has dominated drug discovery approaches in oncology over the same period of time[28]. While TDD and PDD are complimentary drug discovery strategies, PDD can offer some advantages over target based methods, as it allows discovery of potential therapeutics using complex, biological models from heterogeneous, poorly understood disease states[29, 30] and can reveal novel unprecedented therapeutic classes such as the first HDAC inhibitor (vorinostat),

molecular glues (lenalidomide), spicing modulators (risdiplam)[26, 31] and novel conformation-selective binding modes-of-action for existing targets (NXP900/eCF506)[32]. This 'target-agnostic' approach has been greatly assisted by hardware advances in high content microscopy, the development of advanced image analysis software tools and improved phenotypic profiling techniques, such as Cell Painting and Artificial Intelligence/Machine Learning (AI/ML) methods that help classify cell phenotypes and elucidate drug mechanism-of-action[33-36]. Recent advances in multiparametric high-content imaging enables the generation of a phenotypic fingerprint for every chemical (or genetic) perturbation to support the new discipline of 'phenotypic (or morphometric) profiling' that quantifies functional similarities and dissimilarities between drug mechanism-of-action (MOA) within intact cell-based assay systems[33, 37-39]. The Cell Painting assay multiplexes six fluorescent dyes, imaged in five spectral channels to reveal eight broadly relevant cellular components or organelles and can be combined with the development of bespoke automated image analysis pipelines to segment individual cells and calculate thousands of morphological feature-based measurements per cell (e.g. various measures of size, shape, texture, intensity and many others) to produce a data-rich profile that is suitable for the detection of subtle cellular phenotypes which can be linked to biological outcomes[40]. We describe the adaptation and optimization of Cell Painting for profiling compound MOA and target-class across a panel of 6 genetically distinct GSC lines obtained from the Glioma Cellular Genetics Resource (https://github.com/GCGR). Using this approach we provide a comprehensive pharmacological audit of how specific target, pharmacological and chemical classes influence patient-derived GBM cellular phenotypes. We present a large-scale application of this technique using chemically diverse libraries containing FDA approved drugs, or Phase I passed clinical candidates and selective chemical probe compounds against known oncology targets. We identify multiple diverse pharmacological and target classes effective across our genetically distinct panel of patient derived GSCs and present all validated screening hits and their target assignments to the GBM research community. These results support our hypothesis that an unbiased phenotypic led approach, using disease relevant patient derived GSC models and exploitation of deep phenotyping and drug mechanism-of-action profiling technologies is a productive approach to identifying new targets, drug classes and future drug combinations that address the heterogeneity of GBM.

Results

Glioblastoma Stem Cell Models

Patient derived GSCs were obtained from the Glioma Cellular Genetics Resource, and 6 GSC lines were initially selected to cover common transcriptomic subtypes based on their RNA-Seq subtype classification (classical (CLA), mesenchymal (MES), proneural (PRO)). GSC's were cultured on laminin-1 coated substrates, under defined media conditions that have previously been demonstrated to maintain their stem cell like properties[41]. Initial studies demonstrate compatibility with high content imaging (i.e., flat and adherent morphology) and cell number was optimised for 384-well microtiter plate formats to enable high throughput drug screening (Supplementary Figure 1A-C). Given the generally slow growth rates of the GSCs relative to standard cancer cell line cultures, compound exposure over 72 hrs during screening was selected to ensure at least one population doubling in all lines. Short-tandem repeat (STR) profiling was carried out on each GSC line to create reference sequences and all cell lines were expanded and cell stocks banked in liquid nitrogen, to facilitate screening with consistent low passage numbers ensuring minimal biological drift across primary screening and secondary hit validation assays. In order to begin characterising these cell lines, prior to phenotypic screening we examined basal protein expression and post-translational pathway activation status by Reverse Phase Protein Array (RPPA) and cytokine array in 2-dimensional (2D) and 3-dimensional (3D) cell culture conditions. Basal levels of protein and phospho-epitope abundance (in 2D and 3D culture) show functional enrichment of signalling pathways in MAPK, ErbB, VEGF, PI3K-AKT, focal adhesion, EGFR inhibitor resistance and PD-1 checkpoint in cancer (Supplementary Figure 2). The

146 cytokine array profiling further demonstrates enrichment in the secretion of GBM associated
147 chemokine proteins involved in tumour progression, invasion, angiogenesis (IL-6, MMP-7, TIMP1,
148 VEGF), and tumour associated neutrophils (TANs; CCL2, IL-8/CXCL8)[42] including factors previously
149 shown to contribute to GSC subtype trans-differentiation (PRO to MES transition)[43]. (Supplementary
150 Figure 2A-D). Notably the six GSC lines representing three pairs of the common GBM transcriptomic
151 sub-types (CLA, MES and PRO) selected for our study do not cluster into any specific subgroups based
152 on basal protein expression or pathway activation status. Interestingly, high levels of the pro-
153 inflammatory cytokine, interleukin-8 (CXCL8, Supplementary Figure 2C, D) has recently been reported
154 as a druggable target in GBM (*via* humanised anti-IL8 antibody) with an anti-PD-1 combinational
155 blockade[44]. Overall, this pre-screening profiling indicates our proposed GSC drug screening models
156 are representative of typical GBM signalling networks observed in patient samples, express known
157 druggable pathways while capturing the expected broad heterogeneity of GBM tumours at the
158 molecular, protein and morphological levels in both 2D adherent and 3D cell culture.

159 *GSC Cell Painting Assay Development*

160 Previously, we have successfully adapted the Cell Painting protocol[33, 45] to explore drug MOA
161 across cancer cell line panels from diverse lineages including, breast and oesophageal
162 adenocarcinoma[17, 46, 47]. In the current study, we adapt the protocol to our panel of patient-
163 derived GSCs and incorporate live mitochondrial staining prior to fixation and staining with the
164 remaining Cell Painting reagents (Figure 1A, B). It is our understanding that this study describes the
165 first application of phenotypic profiling using the Cell Painting assay to a panel of patient-derived GSC
166 models. Images from each cell line were then used to build a customized CellProfiler image analysis
167 pipeline and confirm appropriate image segmentation and performance of high content analysis. Cell
168 Profiler analysis quantified up to 1006 cellular features from each GSC and principal component
169 analysis was carried out on median aggregated well level data using the StratoMineR HCA platform.
170 Nuclei Count features were also extracted to assess reproducibility of cell seeding in 384-well format
171 and calculate the percentage cell surviving fraction following each compound treatment including
172 signal-to-noise assessment between negative (0.1% (v/v) DMSO) and cytotoxic positive control
173 compounds (paclitaxel, staurosporine). These assay validation studies confirm assay reproducibility
174 and signal-to-noise in 384-well plate formats is suitable for high throughput screening based on
175 industry-standard recommendations[48] (Supplementary Figures 1C & Supplementary Figure 3).

176 Our phenotypic screening campaign performed across the panel of six GSC lines incorporated multiple
177 small molecule compound libraries screened against varied concentrations (ranging from 3-
178 10,000nM) (see methods for specific concentrations for each library & Supplementary Figure 4).
179 Compound libraries included the LOPAC (1280 compounds, Sigma Aldrich), Prestwick FDA (1280
180 compounds), TargetMol L2110 (330 compounds), Structural Genomics Consortium Kinase
181 Chemogenomic set (KCGS – 295 compounds) [49]) and a custom chemogenomic library set (789
182 compounds, 'Comprehensive anti-Cancer small Compound Library, or C^3L[50]) (Table 1). The C^3L
183 library was created with a focus on chemical and known oncology target diversity to functionally
184 evaluate known oncology targets across phenotypic screening assays. The majority of these
185 commercially available compounds (across all library sets) have been through phase I clinical trials. It
186 is our view that this approach presents the potential for discovering novel drug repurposing and drug
187 combination opportunities in addition to identifying new therapeutic targets not previously explored
188 in GBM.

189

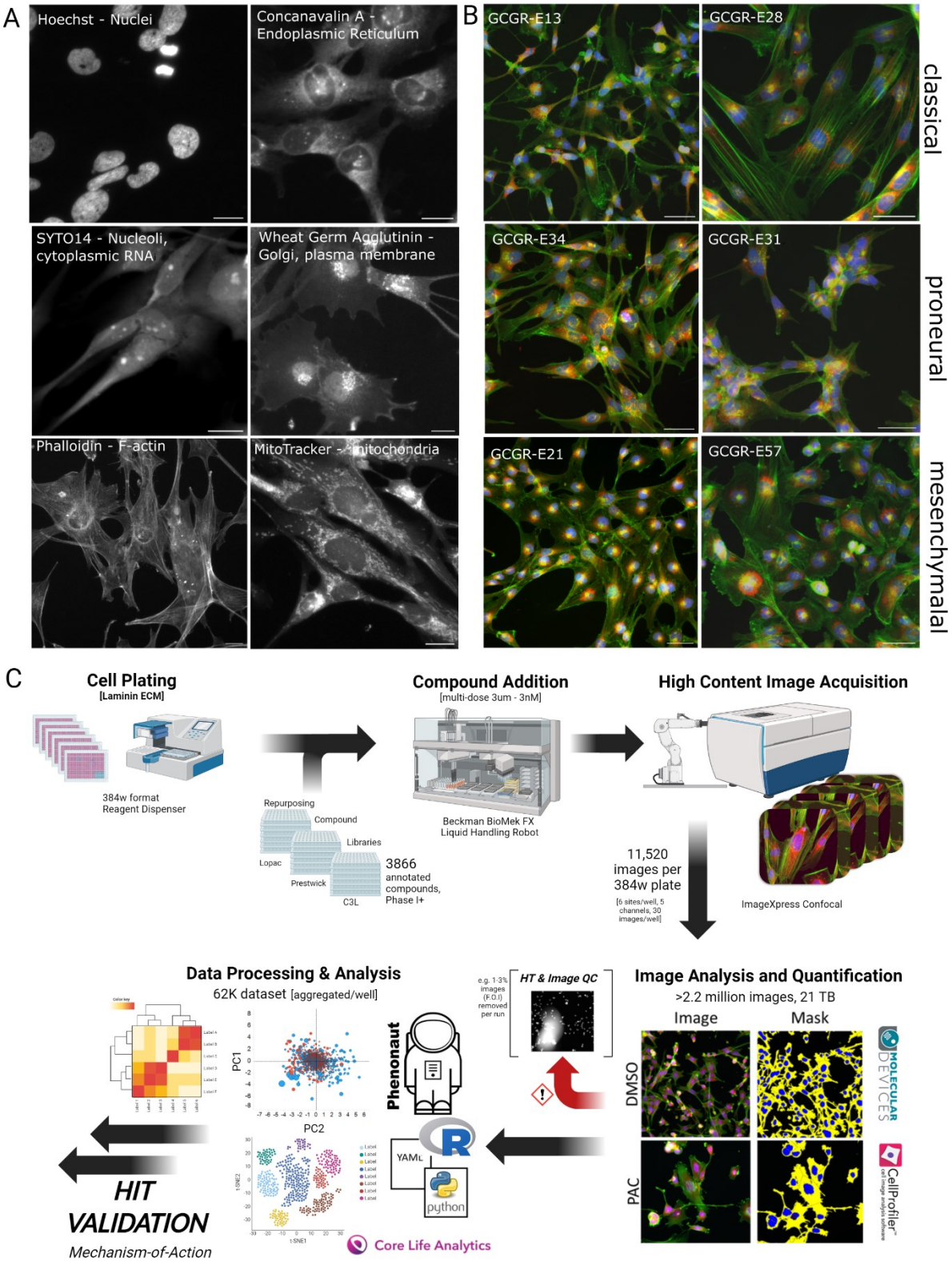

Figure 1. High content phenotypic assay screening workflow on GSC panel. A. Representative image of individual Cell Painting stains (E34 cells) scale bar 20um. B. Representative images of Cell Painting across GSC panel (Hoechst (blue), Phalloidin/WGA (green), Endoplasmic reticulum (red). Scale bar 50um. C. Established high content screening, image and analysis workflow followed by subsequent hit validation and exploration.

High Content Cell Painting Screen, Analysis & Validation

Our optimised GSC high content phenotypic screening and analysis workflow is outlined (Figure 1C) and described in detail in the materials and methods section. Briefly, cell lines were seeded (500-1500

199 cells per well) onto laminin pre-coated 384-well plates, followed by compound addition at 24hrs using
200 automated liquid handling platforms. DMSO (0.1% (v/v)) was used as a negative (compound vehicle)
201 control (48 wells per plate minimum) with staurosporine (1uM) typically used as an assay landmark
202 control for cell death. After 72 hrs compound exposure, cells were subjected to live cell labelling of
203 mitochondria with MitoTracker, followed by fixation, permeabilization, and additional staining with
204 the remaining Cell Painting dyes (see Materials and Methods). Images for phenotypic analysis were
205 acquired using an ImageXpress Confocal high-content microscope with six fields of view (20×
206 objective) over five channels, collecting 11,520 images per 384 well plate. Each compound library was
207 screened separately across all six GCGR cells lines. In total 3,866 compounds were screened (varied
208 doses), ~2.2 million images collected (21 Tb) representing a dataset of >62,000 datapoints. Image
209 analysis was carried out *via* a custom Cell Profiler pipeline and secondary multiparametric data
210 analysis was performed using StratoMineR™ (Core Life Analytics) [51] and TIBCO Spotfire® software
211 (Revvity) see methods. Principal components (PC) 1 and 2 were plotted for LOPAC, Prestwick and C^3L
212 libraries (Figure 2, panels A, C, E) to visualize distribution of active compounds from DMSO controls in
213 phenotypic space. A phenotypic distance metric between each compound and DMSO control was
214 determined using StratoMineR to calculate a normalised Euclidean distance value and then Z score
215 ('Phenotypic Distance Z Score') to rank phenotypic activity of each compound. This phenotypic
216 distance value which identifies compounds having both cytotoxic and non-cytotoxic properties (e.g.
217 morphological changes) was plotted against cell survival (Z-score value of % surviving cells based on
218 nuclei count) to visualise compound effects on both cell morphology and survival (Figure 2, panels B,
219 D, F). Initial hit compound identification was based on two phenotypic criteria, a cell survival threshold
220 (Nuclei Count Z score <-1.95) and phenotypic distance threshold (Z score >1.95) capturing changes in
221 cell number and/or morphology following compound treatment in two or more GSC lines. Hit
222 compounds were triaged by removal of excessive examples of overtly cytotoxic agents (including
223 common anti-cancer agents which have historically been investigated across pan-cancer indications
224 including GBM) such as microtubule disruptors, topoisomerase poisons and proteasome inhibitors and
225 selected hits were taken forward for further investigation.

226 Final quality control checks (compound specific and direct image assessment) were carried out and
227 211 compounds (8.3% hit rate) with phenotypic activity were repurchased from different suppliers
228 from that of the original screening libraries, for validation by dose response testing. Fresh compound
229 stocks, were prepared in 384-well format in a seven-point semi-log dose response (3-3000nM, 40
230 compounds per plate). The validation protocol mirrored the primary screening assay and compound
231 activity (up to 3000nM) upon the primary percentage surviving fraction endpoint was confirmed
232 (validation rate 66%).

233

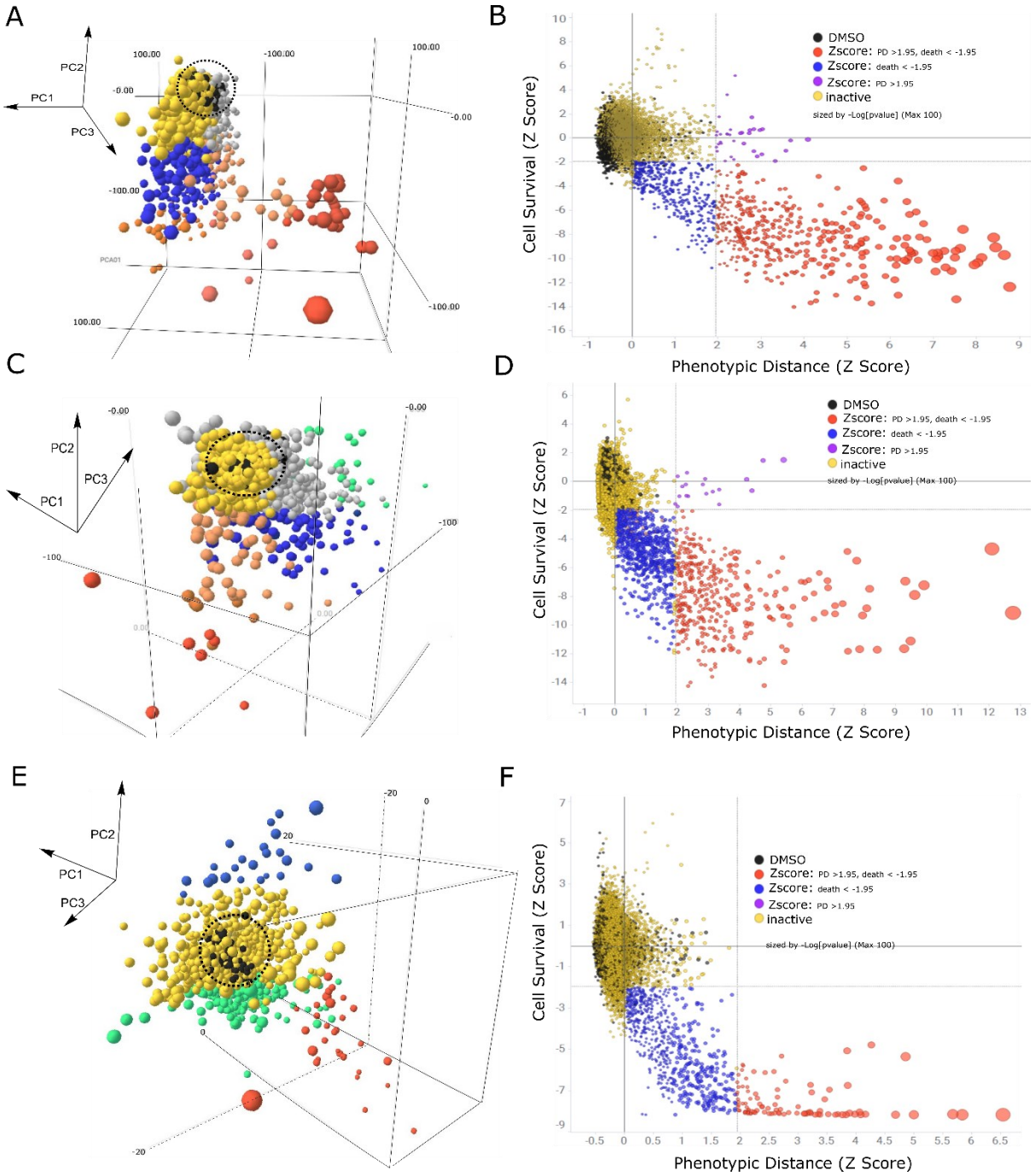

Figure 2. Representative data of high content analysis across 6 GSC lines and three compound libraries. A. Principal component analysis plots (PC1 & PC2) from LOPAC library (strong phenotypes; arbitrary threshold in red), DMSO controls (black) and weaker phenotypes/inactive compounds (yellow), data points sized by compound concentration. B. Cell survival vs phenotypic distance (Z-scores) plots from LOPAC library screen. Significant phenotypic distance (Z score >1.95) and cell death (Z score <-1.95) vs significant cell death (blue, Z score <-1.95) and significant phenotype only (purple, Z score >1.95). Data points sized by -LOG10[p-value]. Corresponding plots are shown in C and D for Prestwick FDA and E and F for the C3L libraries with matching legend.

A

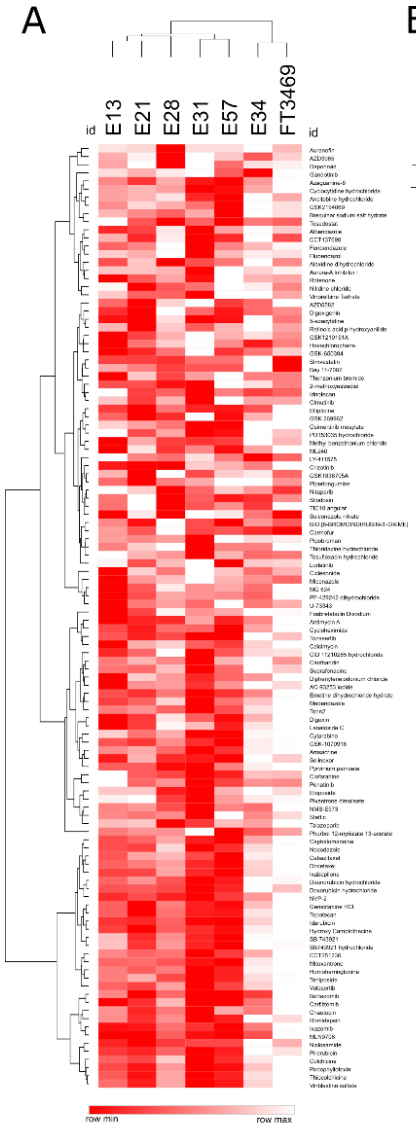

B

Compound	Target(s)	IC50 range (6 GBM lines) (nM)	Comment
Alisertib	AURK	3-20	Broad potency
AZD5582	BIRC3, IAP1/2, XIAP	300	cytostatic, varied
GSK-1324726A	BRD2/3/4	<100	E21, E57 selective
Dinaciclib	CDK1/2/5/9	10	Broad potency
AZD5438	CDK1/2/9	100-500	Broad potency
Abemaciclib	CDK4/6	200	mesenchymal selective
Palbociclib	CDK4/6	100-400	E21, E57, E31 most sensitive
NVP-2	CDK9/cyclinT1	~20	Broad potency
AZD4573	CDK9	~20	Broad potency
Foretinib	c-MET, KDR, FLT4	<500	Broad Potency
CR-1-31-B	EIF4A	5	Broad potency
POM-HEX	ENOL2/1	100-400	E21, E57
Selinexor	exportin-1 (XPO1)	10-200	E28, E31, E57, E13
VS-4718	FAK (PTK2), PYK2	1000	E21, E57 (MEKi combi)
GSK2194069	FASN [P49327]	1000	Broad potency, cytostatic
Fimepinostat	HDAC1/2/3/6/10/11 & PI3K	<100	Broad potency
Emetine	HIF, PDK1, BRD4, ROCK	50-100	Broad potency
NMS-E973	HSP90 (BBB penetrant)	100-300	Broad potency
Gandotinib	JAK2/1, FLT3	100-1000	varied selectivity
SB 743921	KIF11 [KSP]	5-10	Broad potency
GDC-0623	MEK1	10-300	E31, E57, E21 selective
Trametinib	MEK1/2	10-300	E31, E57, E21 selective
Gedatolisib	mTOR, PI3Ka/g	300	Broad potency
Sapanisertib	mTOR (kinase)	100	E31, E57
Daporinad	NAMPT	0.250-4	E28, E34, E31 selective
OTS514	NEK1, TOPK--->ERK	20-200	slight E21, E57 selectivity
PF-03758309	PAK4/6 (pan-PAK)	400-600	varied
AZD5305/Saruparib	PARP1	1-10	E28,E34, E31 Long term assays
Niraparib	PARP1/2	130-300	E28,E34, E31 Long term assays
Talazoparib	PARP1/2	1-10	E28,E34, E31 Long term assays
olaparib	PARP1/2	80-300	E28,E34, E31 Long term assays
Rucaparib	PARP1/2	150-300	E28,E34, E31 Long term assays
CCT251236	PIR (HSF1)	300-1000	Broad potency, cytostatic
GSK-1070916	SIK1 / AURK	300	E57 mostly
AZD3965	SLC16A1 (MCT1)	300	E28, E34 (cytostatic)
Dasatinib	SRC, YES, ABL, c-KIT	<50	E21, E57, E31 most sensitive
Ponatinib	SRC, ABL, PDGFR, VEGFR	100-1000	Broad potency
Bosutinib	SRC, ABL, STAT3, ERK	500-1000	weak overall
eCF506	SRC/FYN/YES	30-150	E21, E57, E31 most sensitive
Saracatinib	SRC/FYN/YES	1000	Broad potency
Pyrvinium pamoate	STAT3	<50	E13, E28, E57, E31
Chaetocin	SUV39H1/EHMT1	5	Broad potency
NXP-800	HSF-1	500-3500	E63, E55
Ganetespib	HSP90	<20	Broad potency
ML240	p97 ATPase	400-1000	E34,E31,E28,E57
Pacritinib	JAK2/1, FLT3	1000-2500	E13, E57
Niclosamide	STAT3	1000-2000	E55

C

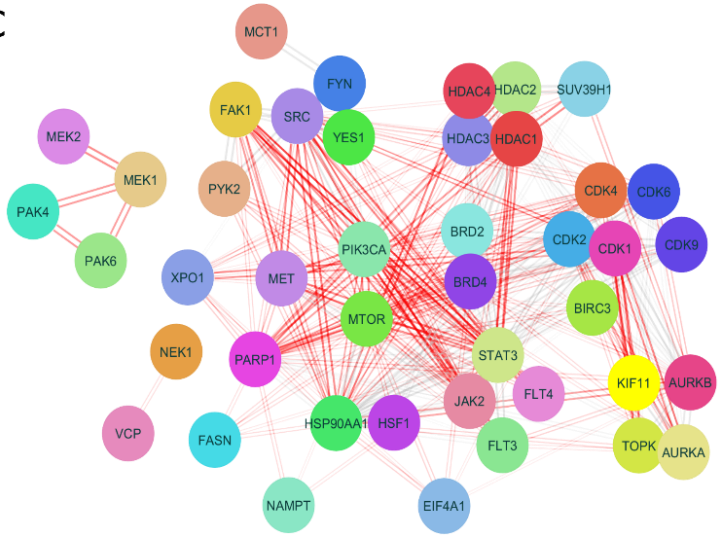

GO Biological Process	Log[FDR]
Protein Kinase activity	-26
Cellular metabolic process	-11
Primary metabolic process	-11
Regulation of apoptosis	-10
Regulation of cell death	-11

KEGG/Wiki Pathways	Log[FDR]
PI3K-AKT Pathway	-8
VEGFA-VEGFR2 signaling	-8
EGF/EGFR signaling pathway	-8
MAPK family signaling cascade	-8
Focal Adhesion	-8
Integrin-mediated cell adhesion	8
Regulation of cell cycle	-8
Cell Cycle, mitotic	-6

Figure 3. Hit validation from primary screening. A. Representative heatmap of normalised Area Under the Curve (nAUC) data from dose response data (normalised nuclei counts) across 6 GSC lines and a normal neuronal stem cell control line (FT3469). Potency (low AUC) is indicated in red (relative scale by row) B. Consolidated, top ranked compounds of interest (in addition to initial validation set) with target annotation, effective dose range and selectivity is indicated. C. STRING-Cytoscape network & enrichment analysis of validated hits, by annotated target(s) search. Go Terms and Log[FDR] from enrichment analysis.

251 In this study, validated compound data lists were generated, including independent phenotypic
252 distance and cell survival assay endpoint lists (Supplementary Table 1 & 2). We have validated our hit
253 compounds primarily via cell survival endpoint (nuclei counts, normalised to DMSO). 159 compounds
254 have been validated in dose response studies (Supplementary Table 1) including 140 compounds
255 originally identified among the 211 hits in the primary screen (66% validation rate) and 19 alternative
256 compounds selected against target classes represented in the hit list. We converted dose response
257 data to Normalised Area Under the Curve (nAUC, scaled between 0-1 with 100% death = 0) for
258 validation ranking (nAUC <0.85 in any line) across the six GSC lines and a normal neuronal stem cell
259 control line (FT3469) to indicate the potential of achieving a therapeutic window (Figure 3A). A
260 consolidated list of validated hit compounds prioritized for further investigation with targets of
261 interest for GBM is listed in Figure 3B. Network analysis of our filtered list, by annotated target(s),
262 demonstrates broad coverage of key target linked pathways, including PI3K-AKT, MAPK, EGFR and
263 adhesion signalling, as well as regulation of cell metabolism, apoptosis and cell cycle/mitosis (Figure
264 3C and Supplementary Figure 5).

265 Initial analysis of the 159 validated compound set (Supplementary table 1) indicates distinct *in vitro*
266 sensitivity of GSCs to topoisomerase poisons, anti-metabolites, proteasome and HDAC inhibitors, as
267 well as particular sensitivity to microtubule targeting agents (taxanes, etc). A prioritized short list (<50
268 compounds) was generated to explore more novel molecular targeted therapies which displayed
269 activity upon GBM and selectivity across a heterogenous GSC panel. Targeted agents of interest
270 involve those targeting cell adhesion (FAK, SRC, YES, FYN), transcription and translation (JAK2/STAT3,
271 CDK9, HDAC, BRD), MAPK pathway/crosstalk (MEK1,2, PAK4,6), DNA damage/repair (PARP, TOPO),
272 mitosis (AURK, KSP), metabolism (FASN, NAMPT) and protein folding/homeostasis (HSP90, HSF, VCP).
273 There is clear chemical and target diversity within this validated hit list, beyond the expected highly
274 potent cytotoxins, which provides a preliminary shortlist for rational drug-target selection and future
275 systematic drug combination strategies. Any such approach would ideally be compatible with current
276 therapy of post-surgical DNA damaging treatments.

277 *Secondary Assays/Sub-validation of target classes: Targeting Transcriptional Regulation*

278 As it is beyond the scope of this article to follow up all of these hits in secondary assays, we have
279 published our full list of validated hit compounds for the GBM research community to explore and
280 perform follow up investigation across similar and alternative GBM models. Within the scope of the
281 current study, we have partially characterised two validated target classes (HDAC and cyclin
282 dependent kinase inhibitors) which demonstrated highly potent (low nM) activity upon GSC survival
283 Supplementary Table 1 and Figure 3).

284 Targeting transcriptional regulation via HDAC inhibitors, we further explored a focussed library of 54
285 structurally distinct HDAC inhibitors by dose-response, as our pilot screening data demonstrated the
286 significant potency of this class of compounds across our GSC panel (e.g., romidepsin, panobinostat)
287 (Figure 4). Commercially available HDAC inhibitors were purchased and 384-well dose response plates
288 were prepared and screened against the same six GSC line panel used for primary screening.
289 Compounds were ranked by potency using the cell survival endpoint (normalised nuclei counts)
290 (Figure 4A). Unsurprisingly, the most potent compounds were pan-HDAC or HDAC1/2 inhibitors,
291 although the top ranked compound (with IC50 values below 50nM across all cell lines) was the dual
292 HDAC/PI3K inhibitor, fimepinostat (CUDC-907). This particular compound is currently undergoing
293 phase II clinical trials in paediatric brain tumours (NCT03893487). Fimepinostat, romidepsin and
294 panobinostat were further validated by performing dose-response and cell cycle analysis (Figure 4B,
295 C, D), which demonstrated G0/G1 accumulation effects on E13 cells over 72 hrs and G2/M arrest in
296 other lines at low nanomolar concentrations (>20nM) (Supplementary Figure 6A, B). Potent induction
297 of apoptosis in GSC lines following treatment with fimepinostat, romidepsin and panobinostat was
298 also confirmed using a kinetic intracellular caspase activity assay (see Figure 6).

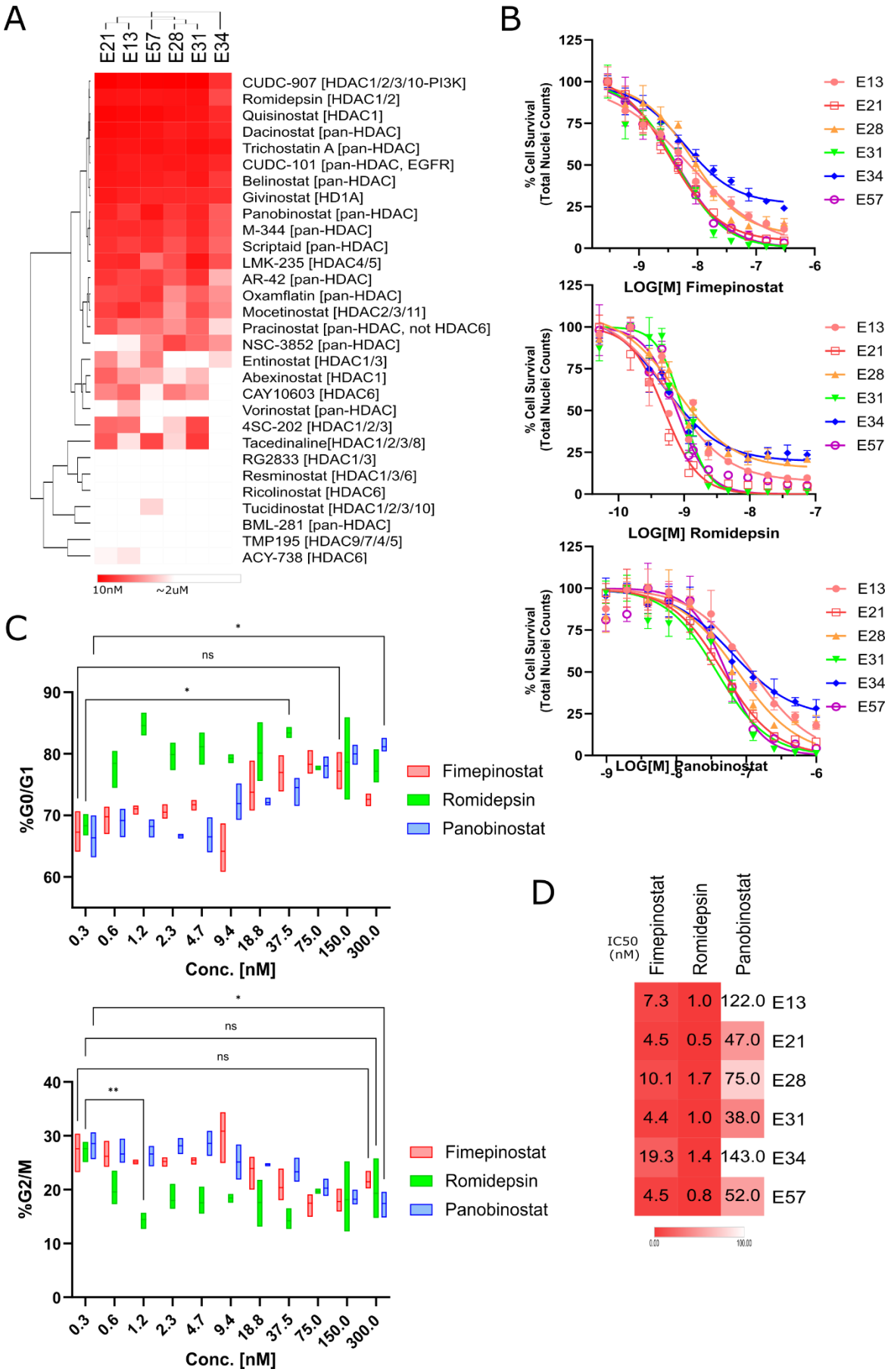

Figure 4. HDAC inhibitor library screening. A. Representative heatmap of IC50 values of HDAC inhibitors on GSC lines. The most potent compounds indicated in red (from 10nM to 2 µM). B Dose response of fimepinostat (CUDC-907)), romidepsin & panobinostat. C. Cell cycle analysis of fimepinostat (CUDC-907)), romidepsin & panobinostat by dose

304 response on E13 cells, from DNA content analysis of Hoechst-stained nuclei. See Supplementary Fig 5 for other cell
305 line cell cycle data. D. IC_{50} values of fimepinostat (CUDC-907)), romidepsin & panobinostat (nanomolar).

306 Romidepsin (4nM), fimepinostat/CUDC-907 (30nM) and panobinostat (200-500nM), induced mostly
307 insignificant/weak G0/G1 accumulation (up to 300nM, Figure 4C & Supplementary Figure 6) and this
308 is in contrast to a gradual but continuous apoptotic signal, starting from >24 hrs (Figure 4E). Phase
309 contrast images show proliferation was not significantly inhibited until ~40 hrs post treatment
310 (compare % confluence of DMSO (black line), Figure 5E) and this appeared independent of
311 proliferation rates (E57 cells doubling time is ~24hrs vs E13 ~60 hrs) but concurrent with inducing
312 apoptosis (compare curve trajectories at 40 hrs, Figure 6A, C vs Figure 6B, D).

313

314 Cyclin dependent kinase inhibitors have been extensively investigated for their anti-cancer activity[52,
315 53] and several CDK inhibitors feature in our validated hit list, including approved CDK4/6 inhibitors
316 abemaciclib and palbociclib. In particular, the CDK9/5/1/2 inhibitor, dinaciclib, as well as the selective
317 CDK9 inhibitor, NVP-2[54], which both show outstanding potency across multiple GSC lines (~20nM
318 IC_{50} across the six GCS lines) (Figure 5A). In addition, a more potent, second generation CDK9 inhibitor,
319 AZD4573, was included in this validation stage and also demonstrated low nM (7-27nM) activity across
320 the 6 GSC lines (Figure 5A).

321 Dinaciclib is a multi-CDK inhibitor which has gained clinical interest in that it targets both cell cycle
322 progression (*via* CDK1/2) and transcription (*via* CDK9), with this 'dual targeting' mode shown to be
323 effective when combined with cisplatin [55, 56]. Validation of dinaciclib, NVP-2 and AZD4573 across
324 our GSC panel indicates broadly cytotoxic profiles (Figure 5A), however, cell cycle analysis of GSC lines
325 treated with a dinaciclib dose response (Figure 5B & Supplementary Figure 6) indicates induction of
326 apoptosis can occur prior to any significant dose dependent cell cycle arrest (see Figure 6E, G) at doses
327 <40nM. This suggests transcriptional dysregulation *via* CDK9 inhibition is having a significant effect
328 upon cell survival, independent of any CDK1/2 inhibition. Overall, AZD4573 has improved potency
329 compared to dinaciclib & NVP-2 (Figure 5A [IC_{50} values] & 5C, compare observable 12nM effects vs
330 DMSO). The effect of selective CDK9 targeting was further examined for time dependent apoptotic
331 induction, proliferation and transcriptomic differential expression (Figures 5 & 6).

332 Induction of apoptosis by CDK9 inhibitors was also monitored *via* kinetic intracellular caspase activity
333 assay of E13 and E57 cells (classical & mesenchymal GSC subtypes). CDK9 inhibitors (20nM) induce a
334 gradually increasing apoptotic signal from ~24hrs after treatment, which starts to accelerate from ~48-
335 72 hrs (Figure 6E, G) while proliferation appears completely halted from Day 0 (Figure 5E), without
336 significant cell cycle effects at this 20nM concentration (Figure 5B & Supplementary Figure 6A, B).

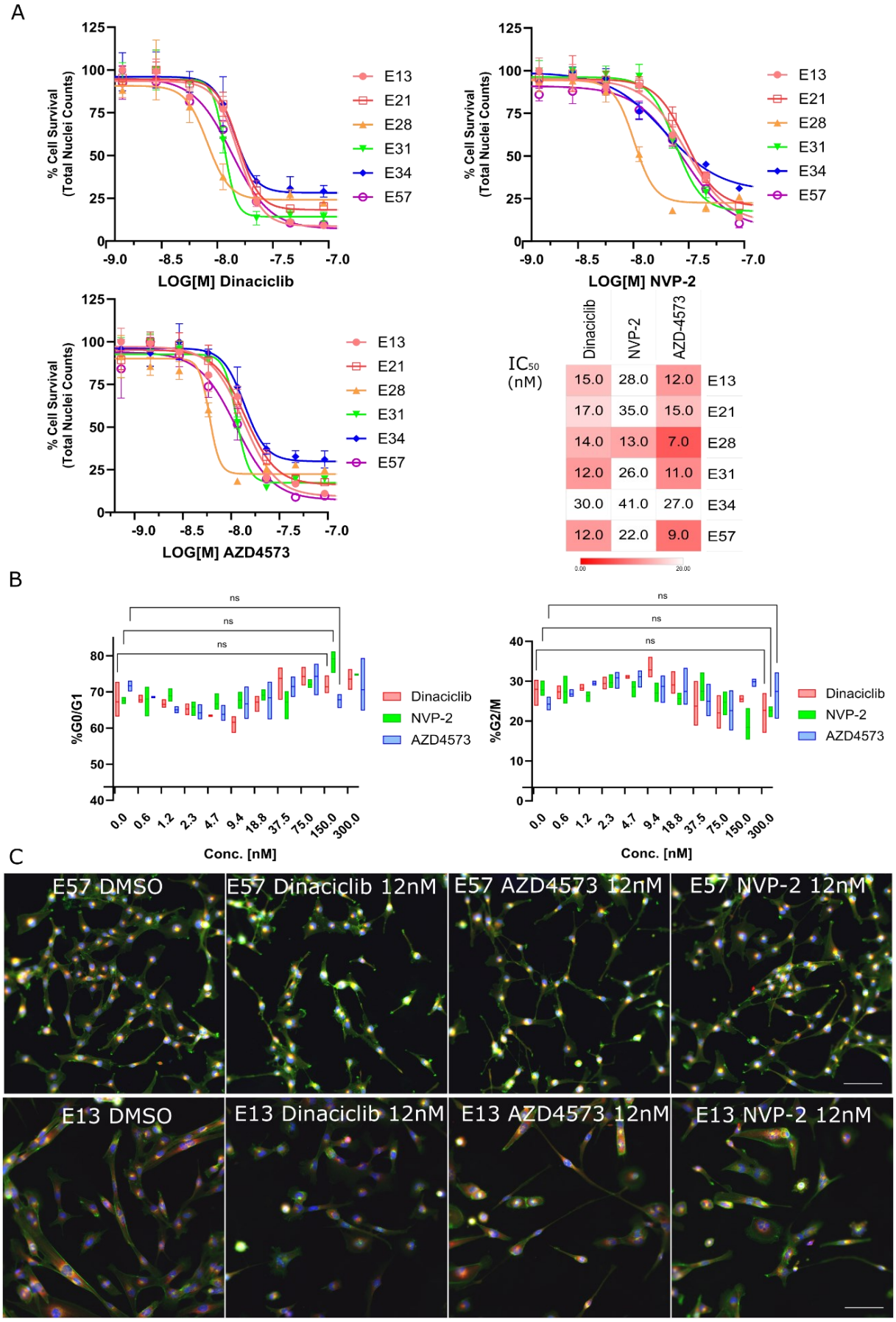

Figure 5. Targeting CDK9 in GBM. A. Dose response validation and IC50 values of Dinaciclib, NVP-2 and AZD4573 shows broad cytotoxic effects across most cell lines. B Cell cycle analysis of E13 cells by dose response shows no significance (two-way ANOVA). See Supplementary Figure 6 for remaining cell cycle effects on other cell lines. Cell cycle analysis from DNA content (Hoechst nuclear stain). D. Representative images of Dinaciclib, AZD4573 and NVP-2 at 12nM vs DMSO on E57 and E13 cells. Scale Bar 100um.

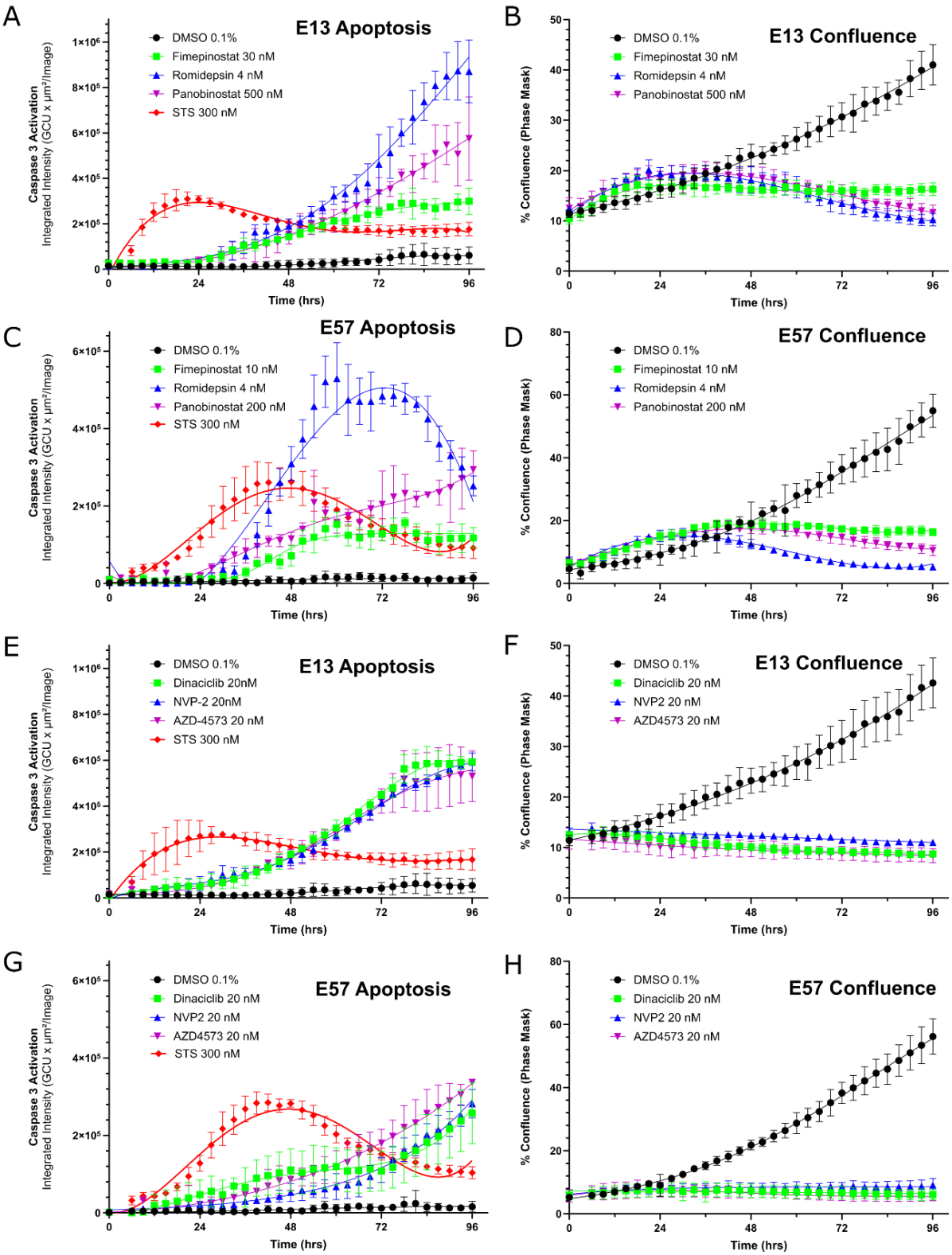

Figure 6. Live cell imaging: Apoptosis & proliferation (confluence) vs time (hrs). E13 (classical) & E57 (mesenchymal) cells were used to characterise the effect of HDAC (romidepsin, panobinostat and fimepinostat) and CDK inhibitors (Dinaciclib, AZD4573, NVP-2) using Nucview-488 Caspase 3/7 detection reagent alongside continuous live cell monitoring using a multi-channel objective.

From these studies it is clear that targeting HDAC and CDK9, and hence transcriptional regulation, is having a cytotoxic benefit against GSCs beyond the usual mechanisms of cell cycle arrest (with the exception of the highly potent molecule, Romidepsin). To further explore the MOA of the CDK inhibitors on GSC lines, we performed NanoString® transcriptomic analysis on sensitive E13 cells that were exposed to 20nM of Dinaciclib, AZD4573 and NVP-2, alongside DMSO controls, for 24 hrs following compound addition. The extracted mRNA was quantified *via* the nCounter™ system (Human Cancer Pathways, 784 genes including controls) and a differential analysis performed (Figure 7). After quality control filtration and removal of housekeeping/control gene sets (post normalisation), 467 genes were available for differential expression & pathway analysis, between untreated and treated cells. Comparison of volcano plots between compounds (Figure 7A) shows suppression of gene expression is prevalent across all three compounds, with dinaciclib and AZD4573 showing similarly stronger effects, relative to NVP-2. The results were further filtered by corrected p-value (Benjamini-Yekutieli FDR). Not surprisingly, a large number of genes (229) were significantly dysregulated across all three compounds (Supplementary Figure 7), with STRING Network analysis (high confidence filter) showing enrichment of KEGG pathways in PI3K-AKT, MAPK and Focal Adhesion Signalling (Supp Figure 5B), among others. Some selective correlation was observed between compound pairs such as AZD4573 & NVP-2 (Figure 7B, C), AZD4573 and Dinaciclib (Figure 7D, E), with further downregulation of gene targets in DNA damage repair, WNT & PI3K signalling. Preliminary combination studies with dinaciclib were performed, combining other top ranked hits romidepsin (pan-HDAC), idarubicin (TOPOII) and ixazomib (proteasome). Combination studies of dinaciclib with romidepsin, idarubicin & ixazomib indicate highly potent additive effects upon GSC survival but not strong synergistic activity (Supplementary Figure 8).

DISCUSSION

The clinical treatment of GBM has not significantly improved median patient survival in more than 20 years, with advances in the genomic characterisation of the disease only highlighting the complexity of the clinical challenge. To address this challenge a number of phenotypic screens of drug libraries and drug combinations performed in complex *ex vivo* or *in vitro* GBM models have recently been reported. However, screens reported to date have been limited in terms of the number of compounds, phenotypic endpoints and the use of use of culture conditions which preserve GBM stem cell characteristics. In this study, our aim was to attempt to address the unmet clinical need in GBM by applying a comprehensive target agnostic, high content phenotypic screen, of thousands of compounds across a well characterized panel of patient-derived GBM stem cell models. The drug libraries were selected to support repurposing of existing oncology drug discovery programs and included Phase I passed or FDA/EMA approved small molecules and drugs with high target selectivity across known oncology targets. We have chosen to not exclusively utilise blood-brain-barrier (BBB)/CNS penetrant drug libraries in order to provide a comprehensive and unbiased evaluation of distinct drug and target classes upon GSC phenotypes. It is our hope that this will be informative towards future medicinal chemistry efforts in generating CNS penetrating small molecules against such targets, or possible incorporation of validated hit compounds into emerging blood-brain-barrier penetrating nanoparticles, designed to effectively deliver drugs and drug combinations administered systemically, directly towards selective tissue and tumour sites including GBM [51-53]. In total 3,866 compounds were screened over multiple concentrations (3– 3000nM), in order to capture the most potent dose-dependent cellular phenotypes beyond simple viability measurements. Our GBM models comprised six heterogeneous, patient-derived GSC lines, representing three of the major transcriptomic subtypes (CLA, MES, PRO). We applied the multiparametric high content 'Cell Painting' assay to screen five drug libraries across the six GSC lines, acquiring over two million images. Image processing and analysis, using software tools such as CellProfiler (cellprofiler.org) and StratoMineR (stratominer.com), identified 211 hit compounds which were re-purchased and validated (66%

validation rate). We provide an updated list of 159 biologically active compounds on human GSC survival and morphology (phenotypic activity) (Figure 3 & Supplementary Table 1 & 2).

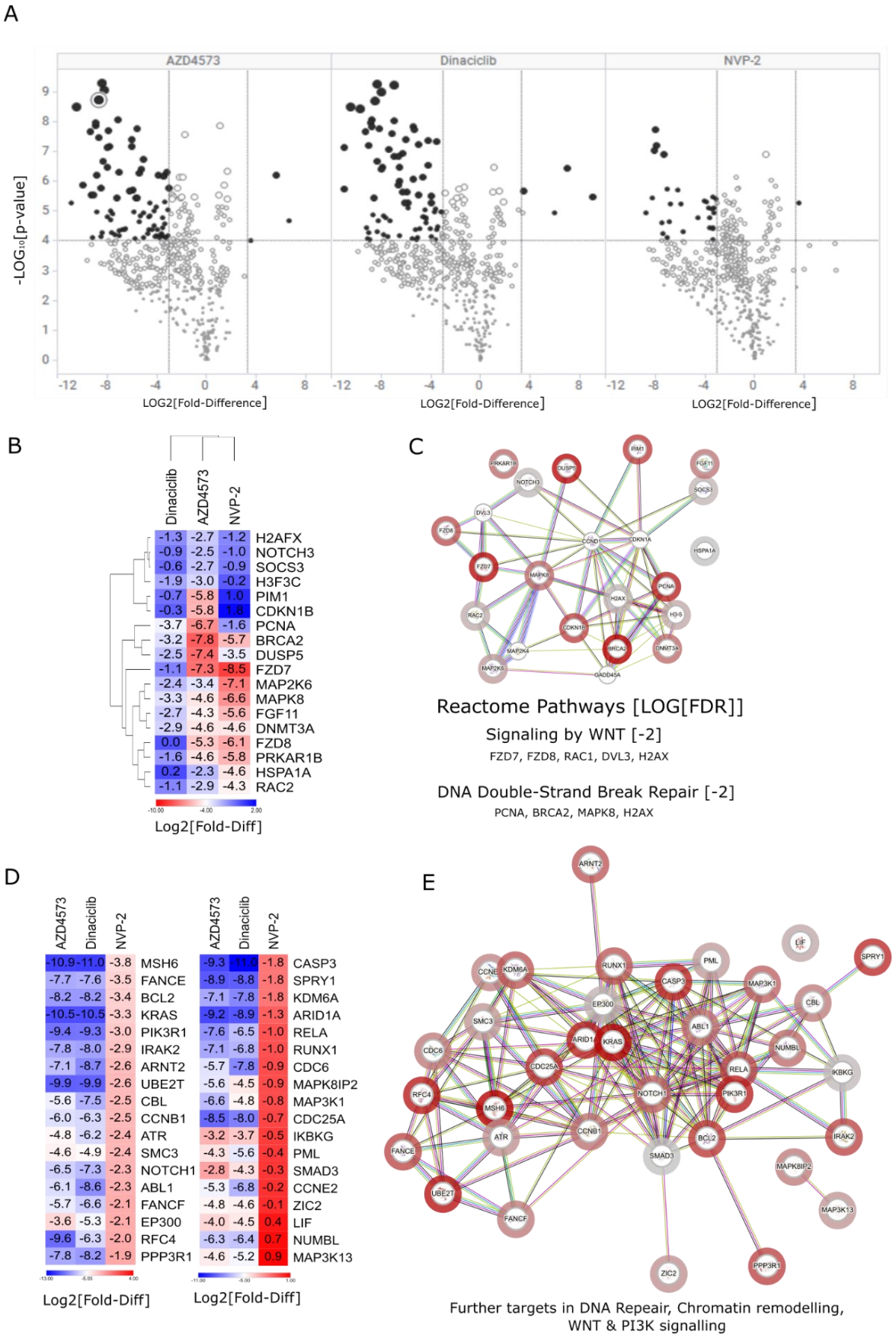

Figure 7. Differential gene expression (DE) analysis of CDK9 inhibitors on E13 cells. A. Volcano plots of DE comparing E13 cells treated with dinaciclib, AZD4573 & NVP-2 versus DMSO. Highly significant/Log2-Fold change highlighted in

black. B, Heatmap of the contrasting DE of NVP-2 and AZD4573 vs dinaciclib. C. Significant differentially expressed genes from CDK9 selective derivatives, AZD4573 & NVP-2, relative to dinaciclib. D, Heatmap of the common DE of AZD5473 & dinaciclib vs NVP-2 E. Significant differentially expressed genes from AZD4573 & dinaciclib only

Common cytotoxic agents, such as microtubule targeting agents, topoisomerase poisons, proteasome and HDAC inhibitors, are prevalent in our hit list and many have previously been investigated in GBM (and other cancers). However, many of these agents have a narrow therapeutic window and significant systemic toxicities limiting their effectiveness. Nevertheless, novel drug delivery technology, such as antibody-cytotoxin conjugates, brain-tumour specific nanoparticles and intra-cranial drug delivery implants, could still utilise such potent molecules clinically in the future. Other molecular targeted compounds identified from our screen, include those targeting cellular adhesion, transcription, DNA damage/repair, cell cycle/mitosis, proliferation, metabolism, and protein folding/homeostasis. The screening deck included a recent, custom made chemogenomic annotated library (Comprehensive Anti-Cancer Compound Library, 'C^3L'[50]), which was designed to incorporate chemical diversity, potency and selectivity on a broad range of oncology targets and thus complements the other "off-the-shelf" commercially available libraries contributing to a comprehensive, relevant and updated pharmacological response profile of patient derived GSCs that we present in this article.

We provide all 159 validated hit compounds demonstrating activity upon GSC survival and morphological endpoints (Supplementary Table 1 & 2) for the GBM research community to explore in further detail. In this article we followed up two drug target classes, HDAC and CDK inhibitors which displayed exquisite low nM activity upon inhibiting cell survival across the heterogeneous panel of GSCs. However, further analysis of the morphological hits (Supplementary Table 2) is likely to also identify compounds that impact upon other GSC phenotypes such as cell cycle, senescence, differentiation and invasion etc.

To further explore the HDAC inhibitor class we screened a library of 54 HDAC inhibitors. Fimepinostat (CUDC-907) was outstandingly the most potent molecule, with <20nM IC_{50} values across the panel. Fimepinostat, a dual PI3K/HDAC inhibitor, is currently undergoing clinical trials for paediatric/young adult brain cancers/solid tumours (NCT03893487), and is a candidate for targeted drug delivery and drug combination strategies. We compared fimepinostat with structurally distinct HDAC inhibitors, romidepsin and panobinostat, by cell cycle and apoptosis assays (Figures 4, 6 & Supplementary Figure 6). While there was a varied response between cell lines (usually more G2/M arrest vs weak G0/G1), there was a common intra-cell line response (and morphology, by live imaging observation) between molecules, suggesting phenotypic activity is most likely mediated through the anti-HDAC activity of fimepinostat rather than its anti-PI3K activity. Indeed, comparison between fimepinostat and potent, selective PI3K inhibitors (all tested at 30nM) demonstrate substantially weaker activity of PI3K inhibition upon GSC proliferation with only the dual PI3K/mTOR inhibitor, gedatolisib, showing any significant effect but still substantially weaker than fimepinostat (Supplementary Figure 9).

Targeting transcriptional regulation has previously been shown to be effective against cancer stem cells (including brain cancers)[57-59], hence we also characterised potent CDK9 inhibitors dinaciclib, NVP-2 (both screening hits) and a more recent selective CDK9 inhibitor, AZD4573. CDK9 is an atypical CDK in that it is a key regulator of RNA Polymerase II (Pol II) transcription initiation, elongation, and termination playing a critical role in transcriptional regulation[60]. Dinaciclib has near equal potency against CDK1/2 (& 5), whereas NVP-2 and AZD4573 are classed as CDK9 selective. AZD4573 has progressed to clinical trials (NCT04630756) and is well tolerated, although CNS penetrance and solid tumour efficacy remains to be determined. Radio-sensitisation of cancer cells with CDK9 inhibitors and drug combinations with DNA damaging agents have previously been reported[61-63], including opportunities in GBM[64]. In our *in vitro* assays, dinaciclib, NVP-2 and AZD4573 are highly potent (7-50nM IC_{50}'s, Figure 5) across GSC lines, immediately antiproliferative with induced cell cycle effects (mostly G2/M arrest at doses >40nM, except for E13 cells, Figure 5, Supplementary Figure 6) and apoptosis taking effect >36 hrs after compound exposure (independent of varied proliferation rates).

456 Differential gene expression analysis (NanoString®) of E13 cells, exposed to CDK9 inhibitors for 24 hrs,
457 reveals highly significant decreases in the expression of genes regulating the cell cycle, DNA damage
458 and repair, anti-apoptosis, PI3K and MAPK signalling across all three compounds (Supplementary
459 Figure 7). MCL-1, an anti-apoptotic BCL2 family member, is a known CDK9 transcriptional and protein
460 target[65]. This probe is not present in the NanoString panel, however, *BCL2* and *BCL2L1* mRNA were
461 downregulated >10 fold, by all three compounds. Genes significantly and selectively decreased by
462 AZD4573 and NVP-2 alone also included Frizzled receptors (*FZD7, FZD8*) and further DNA repair genes
463 in *BRCA2* & *PCNA* (Figure 7B, C). Dinaciclib and AZD4573 also demonstrate a correlative decrease in
464 the same genes (vs NVP-2, Figure 8D, E), particularly *MSH6*, *KRAS, CDC25A* and *ARID1A*. These results
465 indicate that the CDK inhibitors are reprogramming the GSCs into a more vulnerable state, leading to
466 inhibition of cell survival that may be further exploited by combination therapy. Therefore, these
467 results together with previous publications implicating CDK9 as a therapeutic target in GBM suggest
468 targeting CDK9 is worth further exploration in other GBM models and with other drug combinations.

469 Overall, our preliminary screening results presented here serve as a foundation for a systematic
470 approach to the identification, validation and prioritisation of novel therapeutic strategies in GBM
471 including future drug combinations, that could be used concurrently or following standard treatment
472 protocols for GBM. Importantly, we have used patient-derived GSC models, grown under stem-like
473 conditions on a laminin rich ECM scaffold to prioritize follow up investigations of highly potent small
474 molecule active across a genetically distinct and heterogeneous GSC panel. The objective of our
475 phenotypic screening assay was to identify, drug targets and mechanisms-of-action which target
476 heterogeneous GSC phenotypes and thus complements the existing focus on known oncogenic drivers
477 that represent established drug target classes. We anticipate that this approach will identify new
478 therapeutic targets and drug combination hypothesis that target GSC phenotypes rather than
479 individual pathways and thus may be more resilient across heterogeneous patient populations and
480 adaptive drug resistance mechanisms.

481 In conclusions, our high content screening followed by multi-cell line validation across primary and
482 secondary phenotypic assays provides the largest unbiased survey of small molecule therapeutic
483 classes and oncology targets upon GBM stem cell phenotypes that we are aware of. We provide our
484 full lists of validated hits active upon GBM stem cell morphology and cell survival for the research
485 community to explore further. Future studies include expanded screening across larger libraries of
486 compounds to identify novel chemical starting points and novel targets for new GBM drug discovery
487 programs. In addition, further profiling of phenotypic screening hits across a larger number of GBM
488 stem cells lines and integration of phenotypic with molecular data, in order to identify synthetic
489 lethality relationships and or predictive biomarkers of response, will support additional personalized
490 medicine strategies for new drug target classes of GBM. Importantly this unbiased approach can
491 identify new therapeutic opportunities for the majority of GBM patients which do not fall into well-
492 defined subtypes characterized by well-known druggable driver genes thus expanding the scope and
493 inclusion criteria of personalized medicine strategies in GBM.

494

495 ACKNOWLEDGEMENTS

496 This work was funded by a joint Cancer Research UK (C42454/A28596) and The Brain Tumour Charity
497 award (GN-000676) to D.E., N.O.C. and M.C.F. G.M.M and the Glioma Cellular Genetics Resource were
498 supported by the Cancer Research UK (CRUK) Centre Accelerator Award (A21922).

499 CONFLICTS OF INTEREST

500 S.P. is a co-founder, shareholder and Chief Scientific Officer of Trogenix Ltd.

501 N.O.C. is a co-founder, shareholder and management consultant for PhenoTherapeutics Ltd. and

502 N.O.C and M.C.F have held advisory positions and are shareholders in Amplia Therapeutics Ltd.

N.O.C. had patents pertaining to discovery of the SRC/YES1 inhibitor, eCF506/NXP900 (EP3298015B1, JP6684831B2, US10294227B2, CN107849050B, and CA3021550A1) licensed to Nuvectis Pharma.

FUNDING

This work was supported by a Cancer Research UK/Brain Tumour Charity grant C42454/A28596.

508 **[Materials and Methods]**

509 Cell culture

510 Cell lines were obtained from the Glioma Cellular Genetics Resource, Edinburgh and cultured
511 according to optimised conditions for glioma stem cell growth (gcgr.org.uk). Briefly, cells were
512 cultured in DMEM/HAMS-F12 media (Sigma D8437) with B27, N2 supplements (GIBCO 17504-044,
513 17502-048), EGF/FGF (10ng/mL, Peprotech 315-09, 100-18b)) and laminin (4-10ug/mL, Cultrex 3446-
514 005-01). Doubling times are approximately 60 hrs (except E57 cells, db ~24 hrs) with generally low
515 passage ratios to maintain no less than 30% confluence during cell expansion. Cell lines were
516 submitted for STR profiling (ECACC, case number 21579, using a Promega Powerplex 16 HS kit) and
517 were routinely monitored for mycoplasma infection (MycoAlert®, Lonza). All cell lines were expanded
518 and banked in liquid nitrogen (~24 vials each) for continuous turnover of low passage lines during
519 screening. Accutase?

520 Compound screening

521 384 well plates (Greiner Bio-One, uClear, 781091) were precoated in growth media containing
522 10ug/mL laminin (20uL/well) and incubated for 2 hrs at 37 ^{o}C, 5% CO_2 (minimum). Single cell
523 suspensions in growth media were prepared (final seeding densities indicated in Supp Figure 1B, no
524 laminin.) and added to the pre-coated plates (30ul/well, final laminin 4ug/mL). The plates were then
525 incubated for ~20hrs and inspected briefly, prior to compound addition using a Biomek automated
526 liquid handler. Compound library plates (as assay ready daughter plates in 100% DMSO, 10mM-1mM
527 stocks, prepared *via* BioAscent compound management (bioascent.com)) were diluted with media to
528 intermediate plates (1:50, 2% DMSO (v/v)) prior to addition to cells (1:20, final 0.1% DMSO (v/v)).
529 Where required, the intermediate drug plates were further diluted to create reduced dose
530 intermediate plates (with 2% DMSO (v/v)) prior to addition to cells (1:20, final 0.1% DMSO (v/v)).
531 Negative controls (DMSO, 0.1% (v/v), n= 32-48 per plate) and positive controls (staurosporine, 1uM
532 final conc., n= 16) for cell death were added to the intermediate compound plates (up to 320
533 compounds per plate). After the addition of compounds, the plates were then incubated at 37 ^{o}C, 5%
534 CO_2 for 72 hrs.

535 **Table 1: Screening libraries and concentrations used**

Library	# Compounds	Source	Concentrations Used (nM)	Controls (nM)
TargetMol-Anti-Cancer	330	TargetMol #L2110 (2018)	10000, 100, 10, 1nM	Paclitaxel (5nM), Staurosporine (100 nM)
Kinase Chemogenomic Set (KCGS)	187	Structural Genomics Consortium https://cancertools.org/the-kinase-chemogenomic-set-kcgs/	1000, 100 nM	Paclitaxel (5nM), Staurosporine (100 nM)
Prestwick FDA	1280	Prestwick Chemical (~2016) https://www.prestwickchemical.com/screening-libraries/prestwick-chemical-library/	10000, 1000 nM	Staurosporine (1000nM)
LOPAC (Library of Pharmacologically Active Compounds)	1280	Sigma Aldrich	3000, 500 nM	Staurosporine (1000nM)
Comprehensive Anti-Cancer Compound Set C3L	789	Custom (Athanasiadis et al, 2023 iScience **26** (7): 107209.	3000, 300, 30, 3 nM	Staurosporine (1000nM)

536

537 Cell painting

538 Live mitochondrial staining of cells was carried out by the addition of MitoTracker Deep-Red solution
539 (3uM, 10X conc. in media at 5uL/well) using the Integra Viafill automated dispenser. The plates were
540 then incubated for 30 minutes at 37 ^{o}C, 5% CO_2 followed plate cooling and fixation by the addition of
541 16% formaldehyde in PBS (20uL/well – final 4% formaldehyde) using a multidrop combi reagent
542 dispenser. After incubation for 20 minutes, the plates were washed (BioTek plate washer) with PBS

543 and cell painting reagents prepared in 1% BSA/0.01%TX-100 in PBS (Hoechst 33342 5ug/mL, SYTO14
544 3uM, concanavalin A-488 33ug/mL, phalloidin-594 7U/mL or 1:1500, wheat germ agglutinin-594
545 3ug/mL; supplier information below). After washing, PBS was removed and cell painting solution was
546 added using a multidrop combi (20uL/well) followed by incubation at room temperature for 30
547 minutes. The staining solution was then removed and the plates washed with PBS (BioTek) and sealed
548 (Starseal foil seals). The plates were then imaged immediately.

549

Stain	Structure	Wavelength, ex/em (nm)	Channel	Final Concentration	Catalogue No., Supplier
Hoechst 33342	Nuclei	387/447	DAPI	5ug/mL	H1399, Molecular Probes
Concanavalin A Alexa Fluor 488	Endoplasmic reticulum	462/520	FITC	33ug/mL	C11252, Invitrogen
SYTO 14	Nucleoli	531/593	CY3	3 µM	S7576, Invitrogen
Phalloidin Alexa Fluor 594	F-actin	562/624	TxRED	7U/mL (1:1500)	ab176757, Abcam
Wheat germ agglutinin Alexa Fluor 594	Golgi and plasma membrane	562/624	TxRED	3ug/mL	W11262, Invitrogen
MitoTracker DeepRed	Mitochondria	628/692	CY5	300nM	M22426; Invitrogen

550

551 Image acquisition

552 Images were acquired using ImageXpress Confocal high content microscope (Molecular Devices) with
553 automated plate handling (GX series, Peak Analysis and Automation). Exposure settings for each
554 channel were optimised and set. Each well was imaged using a 20× objective and 6 fields of view (30
555 images per well, ~33% well coverage, typically 75-150 cells per image)

556 Image analysis

557 CellProfiler v3.1.5 image analysis software (cellprofiler.org) was used to create a custom analysis
558 pipeline across 5 channels capturing 1155 features per cell. Images were analysed *via* parallel
559 processing using a Unix/Linux high performance computing cluster (University of Edinburgh) and
560 concatenated outputs included median aggregated, well level data. Each completed dataset (library
561 across 6x GCGR lines) was then batch processed using StratoMineR high content analysis platform
562 (stratominer.com). Briefly, stepwise processing in StratoMineR included metadata integration,
563 removal of redundant features (correlation cut-off 0.99, typically 800-850 features remaining), QC and
564 control annotation/flags, normalisation (samples), transformation (Skewness significance 0.0001),
565 feature scaling (robust z score, by plate) and dimensionality reduction (principle component analysis
566 [generalised weighted least squares], Oblique rotation, Ten Berge factor scores method, auto
567 correlation cut-off with ≥20 factors chosen [model based on samples] to represent >60% of data
568 variance [Scree plots]).

569 Processed data was then exported and analysed further using TIBCO Spotfire analysis software
570 (spotfire.com). Hierarchical clustering of normalised datasets was carried out using Morpheus
571 (https://software.broadinstitute.org/morpheus) used in Figures 1,4,5 (complete linkage, Euclidean
572 distance). Network and enrichment analysis of top ~50 annotated compound targets was carried out
573 using STRING[66] & CytoScape (cytoscape.org)[67]

574

575 Live Cell Imaging/Apoptosis Assays

576 GCGR-E13 (1000 cells/well) and GCGR-E57 cells (500 cells/well) were seeded (45uL/well) onto 384w
577 plates (Greiner uClear 781910) pre-coated with 10ug/mL Laminin ECM. After overnight incubation, a
578 solution of NucView-488 reagent (10X conc., 50uM) was added using an Integra ViaFill Liquid dispenser
579 (5uL/well). The compounds were then immediately added using a D300e nanodispenser with back-
580 filling of DMSO to 0.1% (v/v) for all wells, triplicate wells per dose (3 concentrations per compound,
581 based on individual IC50 range). Staurosporine (300nM, 6 replicates per cell line) was used as a

582 positive control for apoptosis induction against DMSO controls (0.1%, 6 replicates per cell line). The
583 plate was then loaded into an IncuCyte S5 Live Cell imager with scans set at 3-hour intervals for 96 hrs
584 (phase and 'green' channels, 10× objective, 1 site). Image processing was carried using IncuCyte in-
585 built analysis modules, with phase area defined as % Confluence/image from the first scan (~t =
586 0+30mins). Apoptosis was quantified from images showing increasing Integrated Intensity from the
587 NucView-488 emission signal (GCU x um^2/Image).

588 Nanostring sequencing/differential analysis

589 mRNA was extracted from E13 cells (~$3x10^6$ cells each condition) after 24 hrs treatment with AZD473,
590 Dinaciclib, NVP-2 (all 20nM) & DMSO (0.1% v/v) in triplicate 10cm dishes, using RNeasy Plus miniprep
591 extraction kit (Qiagen, #74134). Purified mRNA was quantified and diluted to 20ng/uL and submitted
592 for NanoString nCounter analysis against the Human Cancer Pathways Panel (NS_CancerPath_C2535).
593 Samples were hybridised and immediately processed using the nCounter Prep Station and Digital
594 Analyzer (High Sensitivity protocol). QC checks utilised GeNorm to determine most stable reference
595 genes and no QC Flags were raised overall. Differential analysis was carried out on normalised data
596 (normalised to ~20 housekeeping genes) using nSolver™ Analysis Software (version 4.0.70) following
597 standard analysis pipelines. Export data was replotted using TIBCO Spotfire software and also further
598 analysed by hierarchical clustering (https://software.broadinstitute.org/morpheus) and STRING
599 network analysis (string-db.org)[66].

600 Forward-phase protein array: basal cytokine analysis.

601 Conditioned medium was collected after 72 hours incubation. Microarrays were generated using an
602 in-house Aushon BioSystems 2470 array printing platform. The arrays were blocked for 1 hour with
603 SuperG Blocking Buffer (Grace Bio Labs) at room temperature. Conditioned media from glioma stem
604 cell samples were centrifuged at 1000× *g* for 5 minutes at 4 °C. Supernatants were collected and
605 added to microarrays followed by incubation for 12 hours at 4 °C. The arrays were washed three times
606 for 5 minutes in TBS-Tween (0.1% v/v) and blocked for 10 minutes with SuperG Blocking Buffer at
607 room temperature on an orbital shaker, then washed again washed three times for 5 minutes in TBS-
608 Tween (0.1% v/v). Detection antibody mixtures (1:500 antibody dilutions in 5% bovine serum
609 albumin/phosphate buffered saline tween-20 0.1% (BSA/PBST), 1% SuperG Blocking Buffer) were
610 made in microplates. Microarrays were clamped and 50 µL of each antibody was added to
611 corresponding microarray wells. Microarrays were incubated for 1 hour on a flat surface. Clamps were
612 removed and microarrays were washed three times for 5 minutes in TBS-Tween (0.1% v/v).
613 Microarrays were then blocked for 10min with SuperG Blocking Buffer at room temperature and again
614 washed three times for 5 minutes in PBST. Three millilitres (3 mL) of IRDye 800CW Streptavidin (LI-
615 COR Biosciences) was diluted 1:5000 in PBST supplemented with 5% BSA, 1% SuperG Blocking Buffer.
616 Microarrays were covered and incubated with IRDye on a rocker at room temperature for 45 minutes,
617 then washed for 5 minutes, three times in PBST followed by three 5-minute PBS washes and finally
618 washed with distilled water. Microarrays were dried then scanned on the InnoScan 710 high-
619 resolution microarray scanner (Innopsys Life Sciences). The data was normalised for protein
620 concentration and background fluorescence *via* Microsoft Excel templates.

621 Reverse-Phase Protein Array (RPPA): Basal analysis

622 GSC lines were cultured both as mono-layers on laminin-coated cell culture plates and as spheroid
623 cultures on poly-hema coated plates. Cells were set up as mono-layer and spheroid cultures in parallel
624 by seeding equivalent cell numbers from a parental flask with cells in log-phase growth. Cultures were
625 grown until the mono-layer cultures were approximately 70% confluent and then both adherent and
626 suspension cultures were harvested for lysis and preparation for RPPA. For Laminin coating plates
627 were incubated with Laminin at 10ug/ml for 1 hour and then washed with PBS prior to addition of cell
628 lines. Culture media did not contain Laminin and the same media was used for adherent and
629 suspension cultures. For Poly-hema coating plastic 2.4g of poly-hema was dissolved in 200ml of 95%
630 Ethanol and heated to dissolve. The solution was centrifuged at 2500RPM to remove undissolved
631 particles. 4ml was added per 10cm plate (ensuring the plate was completely coated). Plates were left
632 open in a TC hood to air-dry and were rinsed x3 with PBS prior to addition of cells.

633 Mono-layer cultures were washed twice with PBS after removal of media and snap frozen on dry-ice
634 and stored at -80°C. Spheroid cultures were pelleted by centrifugation and washed twice with PBS and
635 then snap frozen and stored until lysis. Cultures were lysed in RIPA buffer supplemented with
636 PhosStop and Complete Mini inhibitor tablets. Lysates were needle syringed five times to ensure
637 complete lysis of cells. Protein quantification was carried out using Coomassie-plus assay
638 (ThermoFisher #23228) and protein concentration was adjusted by to 1 mg/ml. Samples were
639 prepared for printing by addition of 4x Sample buffer and heat denaturation at 95°C for 5 minutes.

640 All samples were diluted to 0.75mg/ml (D1), 0.375mg/ml (D2), 0.1875mg/ml (D3) and 0.09375mg/ml
641 (D4) using PBS containing 10% Glycerol. Array spotting was carried out with the Quanterix 2470
642 Arrayer platform using 185µM pins. Each sample was spotted at four dilutions (D1-D4) onto single pad
643 ONCYTE® SuperNOVA nitrocellulose slides at a 500µM spot-to-spot distance. 168 signalling pathway
644 markers (and appropriate controls) were profiled in a standard RPPA assay as described briefly below.
645 After spotting, the slides were incubated with antigen retrieval solution (1x Reblot strong) for 10 mins
646 before being placed in a microfluidic structure to individually address the arrays with primary or
647 secondary antibody solutions. Following blocking buffer (Superblock T20) for 10 mins the detection of
648 marker antibodies was performed in a two-step sequential assay (1) incubation of an array with
649 primary analyte-specific antibody in blocking buffer for 60 mins at room temperature and (2) removal
650 of excess antibody by washing arrays with PBS-T, followed by a further incubation with blocking buffer
651 and PBS-T washes, and incubation secondary antibody (Dylight-800-labeled anti-species antibodies
652 diluted 1:2500 in Superblock T20) for 30 mins. After further washing and slide drying, the arrays were
653 imaged in the Innopsys Innoscan 710 scanner. Blank signals were determined by omitting the primary
654 antibody from step 1 and instead incubating the array with Superblock T20 alone, followed by step 2.
655 Sample loading on arrays (for normalisation) was determined by staining one slide with fast green
656 protein dye and scanning at 800nm. Microarray images are analyzed using Mapix software (Innopsys).
657 The feature (spot) diameter of the grid was set to 270µm. The average signal intensity is determined
658 for each individual feature and the median background from the adjacent area is subtracted from each
659 feature signal leading to a net signal per feature. Data analysis is performed in a standard way:
660 Fluorescence intensity for each feature on the array is measured. A test is performed for linear fit
661 through the 4 point dilution series for all samples on all arrays using a flag system where R2 > 0.9
662 (green flag) is deemed good, >0.8 (amber flag) is deemed acceptable and <0.8 (red flag) is poor and
663 may be excluded from data analysis. The median values from the 4 point dilution series are calculated
664 and used as a measure of fluorescence intensity. Data is quantified as RFI (relative fluorescence
665 intensity) values relating to relative abundance of total and phosphorylated proteins across the
666 sample set.

667

668

669 **References:**

670

671 1. Philips, A., et al., *Brain Tumours: Rise in Glioblastoma Multiforme Incidence in England 1995-*
672 *2015 Suggests an Adverse Environmental or Lifestyle Factor.* J Environ Public Health, 2018.
673 **2018**: p. 7910754.
674 2. Stupp, R., et al., *Radiotherapy plus concomitant and adjuvant temozolomide for*
675 *glioblastoma.* N Engl J Med, 2005. **352**(10): p. 987-96.
676 3. Dolecek, T.A., et al., *CBTRUS statistical report: primary brain and central nervous system*
677 *tumors diagnosed in the United States in 2005-2009.* Neuro Oncol, 2012. **14 Suppl 5**(Suppl
678 5): p. v1-49.
679 4. Lan, Z., X. Li, and X. Zhang, *Glioblastoma: An Update in Pathology, Molecular Mechanisms*
680 *and Biomarkers.* Int J Mol Sci, 2024. **25**(5).
681 5. Noroxe, D.S., H.S. Poulsen, and U. Lassen, *Hallmarks of glioblastoma: a systematic review.*
682 ESMO Open, 2016. **1**(6): p. e000144.
683 6. Singh, S.K., et al., *Identification of a cancer stem cell in human brain tumors.* Cancer Res,
684 2003. **63**(18): p. 5821-8.

685 7. Singh, S.K., et al., *Identification of human brain tumour initiating cells.* Nature, 2004.
686 **432**(7015): p. 396-401.
687 8. Hemmati, H.D., et al., *Cancerous stem cells can arise from pediatric brain tumors.* Proc Natl
688 Acad Sci U S A, 2003. **100**(25): p. 15178-83.
689 9. Lan, X., et al., *Fate mapping of human glioblastoma reveals an invariant stem cell hierarchy.*
690 Nature, 2017. **549**(7671): p. 227-232.
691 10. Huang, W., et al., *The miR-26a/AP-2alpha/Nanog signaling axis mediates stem cell self-*
692 *renewal and temozolomide resistance in glioma.* Theranostics, 2019. **9**(19): p. 5497-5516.
693 11. Bao, S., et al., *Glioma stem cells promote radioresistance by preferential activation of the*
694 *DNA damage response.* Nature, 2006. **444**(7120): p. 756-60.
695 12. Lathia, J.D., et al., *Cancer stem cells in glioblastoma.* Genes Dev, 2015. **29**(12): p. 1203-17.
696 13. Pietras, A., et al., *Osteopontin-CD44 signaling in the glioma perivascular niche enhances*
697 *cancer stem cell phenotypes and promotes aggressive tumor growth.* Cell Stem Cell, 2014.
698 **14**(3): p. 357-69.
699 14. Wei, W., et al., *Single-Cell Phosphoproteomics Resolves Adaptive Signaling Dynamics and*
700 *Informs Targeted Combination Therapy in Glioblastoma.* Cancer Cell, 2016. **29**(4): p. 563-573.
701 15. Kalisky, T., P. Blainey, and S.R. Quake, *Genomic analysis at the single-cell level.* Annu Rev
702 Genet, 2011. **45**: p. 431-45.
703 16. Mund, A., et al., *Deep Visual Proteomics defines single-cell identity and heterogeneity.* Nat
704 Biotechnol, 2022. **40**(8): p. 1231-1240.
705 17. Hughes, R.E., et al., *Multiparametric High-Content Cell Painting Identifies Copper Ionophores*
706 *as Selective Modulators of Esophageal Cancer Phenotypes.*
707 18. O'Duibhir, E., N.O. Carragher, and S.M. Pollard, *Accelerating glioblastoma drug discovery:*
708 *Convergence of patient-derived models, genome editing and phenotypic screening.* Mol Cell
709 Neurosci, 2017. **80**: p. 198-207.
710 19. Subbiah, V., et al., *Dabrafenib plus trametinib in BRAFV600E-mutated rare cancers: the*
711 *phase 2 ROAR trial.* Nat Med, 2023. **29**(5): p. 1103-1112.
712 20. Raswoli, M., et al., *Salvage chemotherapy after failure of targeted therapy in a child with*
713 *BRAF V600E low-grade glioma.* Pediatr Blood Cancer, 2021. **68**(1): p. e28561.
714 21. Munjapara, V., et al., *BRAF V600E-Mutant Glioblastoma with Extracranial Metastases*
715 *Responsive to Combined BRAF and MEK Targeted Inhibition: A Case Report.* Case Rep Oncol,
716 2022. **15**(3): p. 909-917.
717 22. Miller, K.E., et al., *Clinical response to dabrafenib plus trametinib in a pediatric ganglioglioma*
718 *with BRAF p.T599dup mutation.* Cold Spring Harb Mol Case Stud, 2021. **7**(2).
719 23. Toll, S.A., et al., *Sustained response of three pediatric BRAF(V600E) mutated high-grade*
720 *gliomas to combined BRAF and MEK inhibitor therapy.* Oncotarget, 2019. **10**(4): p. 551-557.
721 24. Newlands, E.S., et al., *Temozolomide: a review of its discovery, chemical properties, pre-*
722 *clinical development and clinical trials.* Cancer Treat Rev, 1997. **23**(1): p. 35-61.
723 25. Moffat, J.G., et al., *Opportunities and challenges in phenotypic drug discovery: an industry*
724 *perspective.* Nat Rev Drug Discov, 2017. **16**(8): p. 531-543.
725 26. Swinney, D.C. and J. Anthony, *How were new medicines discovered?* Nat Rev Drug Discov,
726 2011. **10**(7): p. 507-19.
727 27. Sadri, A., *Is Target-Based Drug Discovery Efficient? Discovery and "Off-Target" Mechanisms*
728 *of All Drugs.* J Med Chem, 2023. **66**(18): p. 12651-12677.
729 28. Moffat, J.G., J. Rudolph, and D. Bailey, *Phenotypic screening in cancer drug discovery - past,*
730 *present and future.* Nat Rev Drug Discov, 2014. **13**(8): p. 588-602.
731 29. Eder, J., R. Sedrani, and C. Wiesmann, *The discovery of first-in-class drugs: origins and*
732 *evolution.* Nat Rev Drug Discov, 2014. **13**(8): p. 577-87.
733 30. Vincent, F., et al., *Developing predictive assays: the phenotypic screening "rule of 3".* Sci
734 Transl Med, 2015. **7**(293): p. 293ps15.
735 31. Vincent, F., et al., *Publisher Correction: Phenotypic drug discovery: recent successes, lessons*
736 *learned and new directions.* Nat Rev Drug Discov, 2022. **21**(7): p. 541.
737 32. Temps, C., et al., *A Conformation Selective Mode of Inhibiting SRC Improves Drug Efficacy*
738 *and Tolerability.* Cancer Res, 2021. **81**(21): p. 5438-5450.

739 33. Bray, M.-A., et al., *Cell Painting, a high-content image-based assay for morphological*
740 *profiling using multiplexed fluorescent dyes.* Nature Protocols, 2016. **11**(9): p. 1757-1774.
741 34. Rohban, M.H., et al., *Systematic morphological profiling of human gene and allele function*
742 *via Cell Painting.* eLife, 2017. **6**: p. e24060-e24060.
743 35. Cimini, B.A., et al., *Optimizing the Cell Painting assay for image-based profiling.* bioRxiv,
744 2022: p. 2022.07.13.499171-2022.07.13.499171.
745 36. Way, G.P., et al., *Evolution and impact of high content imaging.* SLAS Discov, 2023. **28**(7): p.
746 292-305.
747 37. Caie, P.D., et al., *High-content phenotypic profiling of drug response signatures across*
748 *distinct cancer cells.* Mol Cancer Ther, 2010. **9**(6): p. 1913-26.
749 38. Bray, M.A., et al., *A dataset of images and morphological profiles of 30 000 small-molecule*
750 *treatments using the Cell Painting assay.* Gigascience, 2017. **6**(12): p. 1-5.
751 39. Perlman, Z.E., et al., *Multidimensional drug profiling by automated microscopy.* Science,
752 2004. **306**(5699): p. 1194-8.
753 40. Gustafsdottir, S.M., et al., *Multiplex Cytological Profiling Assay to Measure Diverse Cellular*
754 *States.* PLoS ONE, 2013. **8**(12): p. 80999-80999.
755 41. Pollard, S.M., et al., *Glioma stem cell lines expanded in adherent culture have tumor-specific*
756 *phenotypes and are suitable for chemical and genetic screens.* Cell Stem Cell, 2009. **4**(6): p.
757 568-80.
758 42. Codrici, E., et al., *Friends with Benefits: Chemokines, Glioblastoma-Associated*
759 *Microglia/Macrophages, and Tumor Microenvironment.* Int J Mol Sci, 2022. **23**(5).
760 43. Fedele, M., L. Cerchia, and S. Battista, *Subtype Transdifferentiation in Human Cancer: The*
761 *Power of Tissue Plasticity in Tumor Progression.* Cells, 2024. **13**(4).
762 44. Liu, H., et al., *Neutralizing IL-8 potentiates immune checkpoint blockade efficacy for glioma.*
763 Cancer Cell, 2023. **41**(4): p. 693-710 e8.
764 45. Bray, M.-A. and A.E. Carpenter, *Quality Control for High-Throughput Imaging Experiments*
765 *Using Machine Learning in Cellprofiler.* Methods in molecular biology (Clifton, N.J.), 2018.
766 **1683**: p. 89-112.
767 46. Hughes, R.E., et al., *High-Content Phenotypic Profiling in Esophageal Adenocarcinoma*
768 *Identifies Selectively Active Pharmacological Classes of Drugs for Repurposing and Chemical*
769 *Starting Points for Novel Drug Discovery.* SLAS Discovery, 2020. **25**(7): p. 770-782.
770 47. Warchal, S.J., et al., *High content phenotypic screening identifies serotonin receptor*
771 *modulators with selective activity upon breast cancer cell cycle and cytokine signaling*
772 *pathways.* Bioorg Med Chem, 2020. **28**(1): p. 115209.
773 48. Markossian, S., et al., *Assay Guidance Manual for Drug Discovery: Robust or Go Bust.* SLAS
774 Discov, 2021. **26**(10): p. 1241-1242.
775 49. Wells, C.I., et al., *The Kinase Chemogenomic Set (KCGS): An Open Science Resource for Kinase*
776 *Vulnerability Identification.* Int J Mol Sci, 2021. **22**(2).
777 50. Athanasiadis, P., et al., *Chemogenomic library design strategies for precision oncology,*
778 *applied to phenotypic profiling of glioblastoma patient cells.* iScience, 2023. **26**(7): p. 107209.
779 51. Omta, W.A., et al., *HC StratoMineR: A Web-Based Tool for the Rapid Analysis of High-Content*
780 *Datasets.* Assay Drug Dev Technol, 2016. **14**(8): p. 439-452.
781 52. Asghar, U., et al., *The history and future of targeting cyclin-dependent kinases in cancer*
782 *therapy.* Nat Rev Drug Discov, 2015. **14**(2): p. 130-46.
783 53. Zhang, M., et al., *CDK inhibitors in cancer therapy, an overview of recent development.* Am J
784 Cancer Res, 2021. **11**(5): p. 1913-1935.
785 54. Olson, C.M., et al., *Pharmacological perturbation of CDK9 using selective CDK9 inhibition or*
786 *degradation.* Nat Chem Biol, 2018. **14**(2): p. 163-170.
787 55. Howard, D., et al., *Dinaciclib as an effective pan-cyclin dependent kinase inhibitor in platinum*
788 *resistant ovarian cancer.* Front Oncol, 2022. **12**: p. 1014280.
789 56. Howard, D., et al., *Dinaciclib, a Bimodal Agent Effective against Endometrial Cancer.* Cancers
790 (Basel), 2021. **13**(5).
791 57. Garros-Regulez, L., et al., *Targeting SOX2 as a Therapeutic Strategy in Glioblastoma.* Front
792 Oncol, 2016. **6**: p. 222.

793 58. Zhang, Z. and Y. Zhang, *Transcriptional regulation of cancer stem cell: regulatory factors*
794 *elucidation and cancer treatment strategies.* J Exp Clin Cancer Res, 2024. **43**(1): p. 99.
795 59. Singh, D.K., et al., *Oncogenes Activate an Autonomous Transcriptional Regulatory Circuit*
796 *That Drives Glioblastoma.* Cell Rep, 2017. **18**(4): p. 961-976.
797 60. Bacon, C.W. and I. D'Orso, *CDK9: a signaling hub for transcriptional control.* Transcription,
798 2019. **10**(2): p. 57-75.
799 61. Veeranki, O.L., et al., *Targeting cyclin-dependent kinase 9 by a novel inhibitor enhances*
800 *radiosensitization and identifies Axl as a novel downstream target in esophageal*
801 *adenocarcinoma.* Oncotarget, 2019. **10**(45): p. 4703-4718.
802 62. Orhan, E., et al., *CDK inhibition results in pharmacologic BRCAness increasing sensitivity to*
803 *olaparib in BRCA1-WT and olaparib resistant in Triple Negative Breast Cancer.* Cancer Lett,
804 2024. **589**: p. 216820.
805 63. Cao, S., et al., *Inhibition of CDK9 induces apoptosis and potentiates the effect of cisplatin in*
806 *hypopharyngeal carcinoma cells.* Biochem Biophys Res Commun, 2017. **482**(4): p. 536-541.
807 64. Ranjan, A., et al., *Targeting CDK9 for the Treatment of Glioblastoma.* Cancers (Basel), 2021.
808 **13**(12).
809 65. Cidado, J., et al., *AZD4573 Is a Highly Selective CDK9 Inhibitor That Suppresses MCL-1 and*
810 *Induces Apoptosis in Hematologic Cancer Cells.* Clin Cancer Res, 2020. **26**(4): p. 922-934.
811 66. Szklarczyk, D., et al., *The STRING database in 2023: protein-protein association networks and*
812 *functional enrichment analyses for any sequenced genome of interest.* Nucleic Acids Res,
813 2023. **51**(D1): p. D638-D646.
814 67. Shannon, P., et al., *Cytoscape: a software environment for integrated models of biomolecular*
815 *interaction networks.* Genome Res, 2003. **13**(11): p. 2498-504.

816